

# Evaluating the Ultimate Bearing Capacity of Glued Laminated Bamboo Hollow Columns under Eccentric Compression

Yi Su,\* Jun Zou, and Wei Lu

To improve the utilization rate of bamboo, glued laminated bamboo hollow column (GLBHC) was examined under eccentric compression to study the effects of different slenderness ratios, eccentric distances, and wall thicknesses on its ultimate bearing capacity. The nonlinear deformation of the material and the P-delta effect of the column occur under eccentric compression, which can affect its ultimate bearing capacity, so it is very important to analyze the elastic-plastic buckling of the column. Moreover, the discontinuity of the hollow column section aggravates the nonlinear deformation. To accurately estimate the ultimate bearing capacity of GLBHC, considering the difference in tensile and compression elastic modulus, two eccentric compression models were established. A formula for ultimate bearing capacity of the GLBHC under eccentric compression was proposed, and the calculated results were in good agreement with the test results.

DOI: 10.15376/biores.17.3.5372-5392

*Keywords:* Laminated bamboo lumber; Hollow column; Eccentric load; Inelastic analysis; Ultimate bearing capacity

*Contact information:* School of Civil Engineering, Nanjing Forestry University, Jiangsu, 210037, China;  
*\*Corresponding author:* [suyi@njfu.edu.cn](mailto:suyi@njfu.edu.cn)

## INTRODUCTION

As an eco-friendly and sustainable new material, laminated bamboo lumber (LBL) has been developed for building structures due to its strong mechanical properties and stability (Mena *et al.* 2012; Yao *et al.* 2019; Dauletbek *et al.* 2021), and the durability of these materials far exceeds that of raw bamboo (Varela *et al.* 2013; Guan *et al.* 2018). However, the columns cannot be ensured completely in the axial compression stage in building structures. For example, many high-rise buildings, frame columns, trusses of the roof, and support columns of bridges are always under eccentric compression, which is true in general for beam-columns (Danesh and Mohammadrezapour 2018; Sui *et al.* 2018; Hu *et al.* 2020; Tan *et al.* 2020). The bending deformation under eccentric loads can affect its ultimate bearing capacity, and the nonlinear deformation reduces it further.

Many studies have been carried out on the mechanical properties of bamboo columns under axial and eccentric compression. Bahtiar *et al.* (2021) conducted an axial compression test on 190 *Guadua* columns with different slenderness ratios and found that its ultimate bearing capacity decreases with the slenderness ratio increasing. Moreover, the failure modes of the columns with different slenderness ratios were different (Li *et al.* 2016). The ultimate bearing capacity is determined by the buckling critical load in the elastic or inelastic state, which was summarized by 40 parallel bamboo strand lumber

columns (PBSLs) tests (Cheng *et al.* 2020). Nie *et al.* (2021) reported that the ultimate bearing capacity of the bamboo columns under axial load was related to slenderness ratios, cross-sectional area, and diameter thickness, and proposed a bearing capacity prediction model. Li *et al.* (2016) conducted an eccentric compression test on 35 LBL columns and found that eccentric distance is the main factor for the decrease of their ultimate bearing capacity. The ultimate bearing capacity of the column is affected in an obvious manner by eccentricity (Cheng *et al.* 2022). Zhou *et al.* (2021) found that the ultimate bearing capacity of wooden columns reinforced by BFRP can be obviously affected by different eccentric distances, and predicted its ultimate bearing capacity by using the finite element method. Wang *et al.* (2018) studied the elastic and elastoplastic buckling behavior of laminated bamboo columns under axial and eccentric compression. However, in comparison with solid columns, very little research is available for the hollow columns, unfortunately. The stiffness of a hollow column is greater than that of a solid column under the same cross-sectional area. Harries *et al.* (2000) have proposed a box-section glued hollow wooden column and found that its bearing capacity under the same cross-section area is higher than that of the solid column. AlAjarmeh *et al.* (2019) have reported that the hollow column with GFRP reinforcement has a large stiffness and better resistance to lateral deformation. Zhu *et al.* (2021) have studied that when the material of the same volume, the length, and eccentricity of the column are equal, the bearing capacity of the hollow column is higher than that of the solid column, and the stiffness of the resistance to lateral deformation is significantly increased. In sum, the hollow column has better stability and ultimate bearing capacity.

The failure modes of the hollow column under eccentric compression are different from that of a solid column. The elastoplastic deformation in the bending direction is more obvious than that of the solid column, which is caused by the discontinuities in cross-sections. During the eccentric loading process, the local degumming and cracking failures will occur at the glued connections of the plates (Wang *et al.* 2019; Liu *et al.* 2020), the buckling deformation of the plywood on the compressive side will occur (Wu *et al.* 2014), and even the external drum phenomenon will occur (Zhao *et al.* 2017), which will significantly reduce its ultimate bearing capacity. Therefore, it is necessary to propose a calculation method to evaluate the ultimate bearing capacity.

This study focused on the elastoplastic buckling behavior of GLBHC under eccentric compression. The failure modes were analyzed and the effects of slenderness ratios, eccentric distances, and wall thicknesses on its ultimate bearing capacity were studied. Taking the strains of the tensile and compressive side to reach the ultimate strain as the failure criterion and assuming cross-sectional strain complies with the flat section assumption, the models under the eccentric compression were established based on the theory of elastic small deformation. A formula for estimating the ultimate bearing capacity of GLBHC under eccentric compression is proposed.

## EXPERIMENTAL

### Materials

The GLBHC is made of LBL from the same factory in Fujian, China. The mechanical properties of LBL are very important to the ultimate bearing capacity of the GLBHC under eccentric compression. Therefore, the mechanical properties of LBL were tested according to ASTM D143 (2022), and 30 samples were measured for each group to

find their average values. The mechanical properties including compression strength parallel to the grain, tensile strength, and elastic modulus are shown in Table 1. The simplified stress-strain model is shown in Eq. 1, and the curve is shown in Fig. 2.

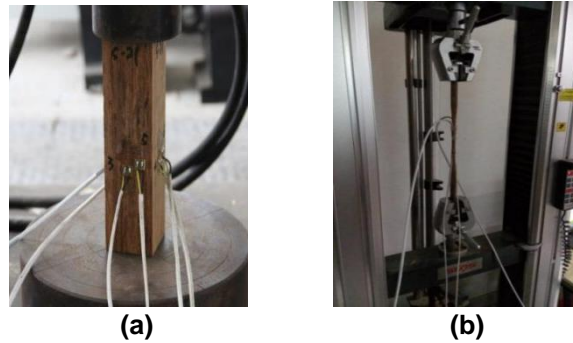


**Fig. 1.** Test set up: (a) longitudinal compression; (b) longitudinal tensile

**Table 1.** Mechanical Properties of LBL

Types of tests	Compression					Tensile		
	$\sigma_{cu}$ /(MPa)	$\sigma_{ce}$ /(MPa)	$\epsilon_{cu}$	$\epsilon_{ce}$	$E_c$ /(GPa)	$\sigma_{tu}$ /(MPa)	$\epsilon_{tu}$	$E_t$ /(GPa)
Parallel to the Grain	59.36	36.57	0.0179	0.0033	116.13	119	0.0118	100.85
Standard deviation	4.980	2.690	0.001	0.002	1.010	8.920	0.002	0.942
Coefficient of variation	7.50%	3.41%	5.34%	4.37%	8.47%	6.42%	3.34%	7.34%

Note:  $E_c$  is the compressive elastic modulus,  $E_t$  is the tensile elastic modulus,  $\sigma_{ce}$  is the proportional ultimate stress,  $\epsilon_{ce}$  is the proportional ultimate compressive strain,  $\sigma_{cu}$  is the ultimate compressive stress,  $\epsilon_{cu}$  is the ultimate compressive strain, and  $\epsilon_{tu}$  is the ultimate tensile strain. When the compressive stress drops to 85% of the ultimate compressive stress, it can be considered that the specimen was broken, and its corresponding compressive stress is expressed by  $\sigma'_c$ , and its value is 50.46Mpa, and the compressive strain is expressed by  $\epsilon_m$ , and its value is 0.027.

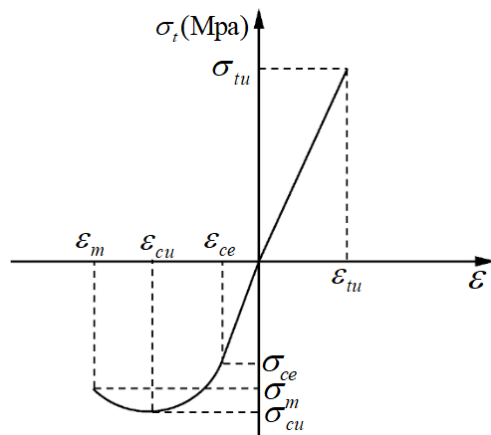


**Fig. 2.** Simplified model of stress-strain

$$\sigma(\varepsilon) = \begin{cases} 10085\varepsilon & 0 \leq \varepsilon \leq \varepsilon_{tu} \\ 11613\varepsilon & -\varepsilon_{ce} \leq \varepsilon \leq 0 \\ 102653\varepsilon^2 + 3675\varepsilon - 26.5 & -\sigma'_c \leq \varepsilon \leq -\varepsilon_{ce} \end{cases} \quad (1)$$

### Specimens Design

The four LBL plates were spliced into GLBHC with phenol glue. For the production of GLBHC, 4- to 5-year-old bamboo culms were selected and divided into strips (Chen *et al.* 2014). The strips (5 mm) were dried until the moisture content was reduced to 10% (Sharma *et al.* 2015). The LBL plate was sanded several times to remove wax and silica from both sides, which can achieve a uniform size of the strips (Assima *et al.* 2021). The strips were treated with carbonization or bleaching (Li *et al.* 2016). Finally, the bamboo plates were made into GLBHC using hot pressing and high-temperature treatment, and a compression of 1 MPa was applied at a temperature of 120 °C for 2 h by the pressure machine (LY200x16-250/5), and the section size of the hollow column is shown in Fig. 3.

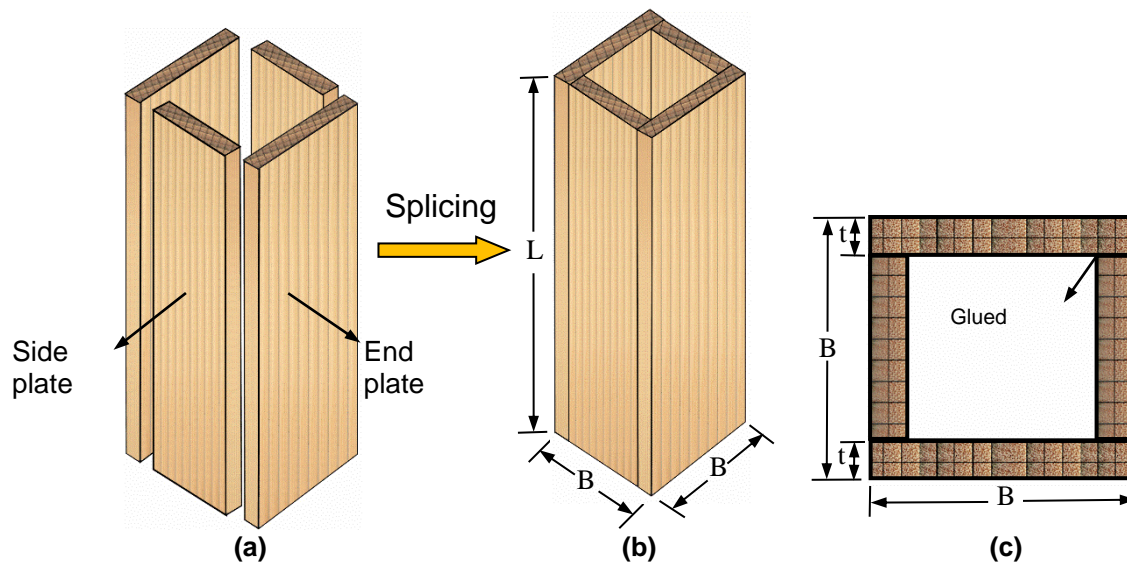


**Fig. 3.** Section size of hollow column: (a) split view, (b) overall view, and (c) top view

Equation 2 was used to calculate the slenderness ratio is  $\lambda=l/i$ , where  $l$  is the length of columns and  $i$  is the rotation radius of cross-section. Because the section of the GLBHC is a square, the rotation radius in both directions is the same.

$$i = \sqrt{\frac{I}{A}} = \sqrt{\frac{B^2 + (B - 2t)^2}{12}} \quad (2)$$

where  $I$  is the cross-sectional moment of inertia,  $A$  is the area of the cross-section,  $B$  is the width of the section, and  $t$  is the wall thickness.

The critical slenderness ratio can be calculated by the formula (Chen *et al.* 2020),

$$\lambda_{cr} = \pi \sqrt{\frac{E_1}{\sigma_{ce}}} = \pi \sqrt{\frac{11613}{36.57}} = 56 \quad (3)$$

where  $\lambda > 56$  is called a long column,  $17 < \lambda < 56$  is called an intermediate column, and  $\lambda < 17$  is called a short column (2005).

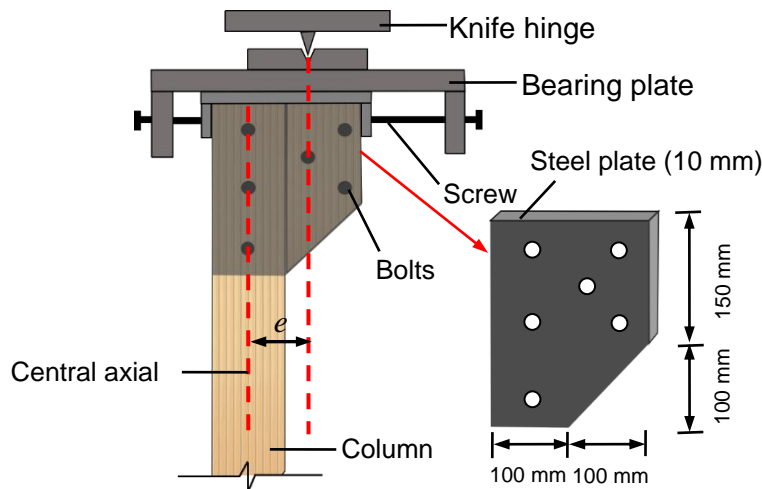
The eccentric distances of the specimen were designed according to GB/T50329 (2012). The bamboo brackets are set at both ends of the specimen to withstand the eccentric load. The bamboo brackets are connected to the specimen with two steel plates and reinforced by bolts, which can prevent the bamboo brackets from being damaged under eccentric load. The mechanical properties of GLBHC with different slenderness ratios, eccentric distances, and wall thickness under eccentric compression were determined. The specific size and number of specimens are shown in Table 2.

**Table 2.** Dimensions and Eccentricities of the Tested Columns

Specimens	$L/mm$	$B/mm$	$t/mm$	$e/mm$	Slenderness ratio
1350-40	1350	100	20	40	40
1350-80	1350	100	30	80	40
1350-120	1350	100	40	120	40
1650-40	1650	100	20	40	49
1650-80	1650	100	30	80	49
1650-120	1650	100	40	120	49
1950-40	1950	100	20	40	58
1950-80	1950	100	30	80	58
1950-120	1950	100	40	120	58

### Loading Procedure and Instrumentation

The test was conducted on an electro-hydraulic servo universal testing machine (Jinan Xinguang Testing Machine Manufacturing, Jinan, China) with a capacity of 500 kN, a TDS-530 data acquisition instrument, and linear variable differential transformers (LVDTs). The specimen was installed vertically on the testing setup, and both ends were placed on the knife hinge support, as shown in Fig. 4.



(a)

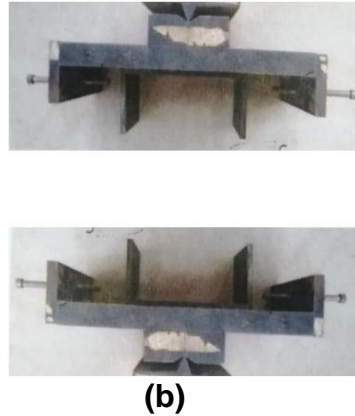


**Fig. 4.** Diagram of the knife hinge: (a) components of a knife hinge; (b) actual knife hinge

The load was transmitted to the steel plate through the knife hinge and then to the specimen. The eccentric distance can be changed by adjusting the screws on both sides, as shown in Fig. 5. The speed of loading was 2 mm/min, and the test continued until the specimen was broken or the load dropped to 85% of the peak load.

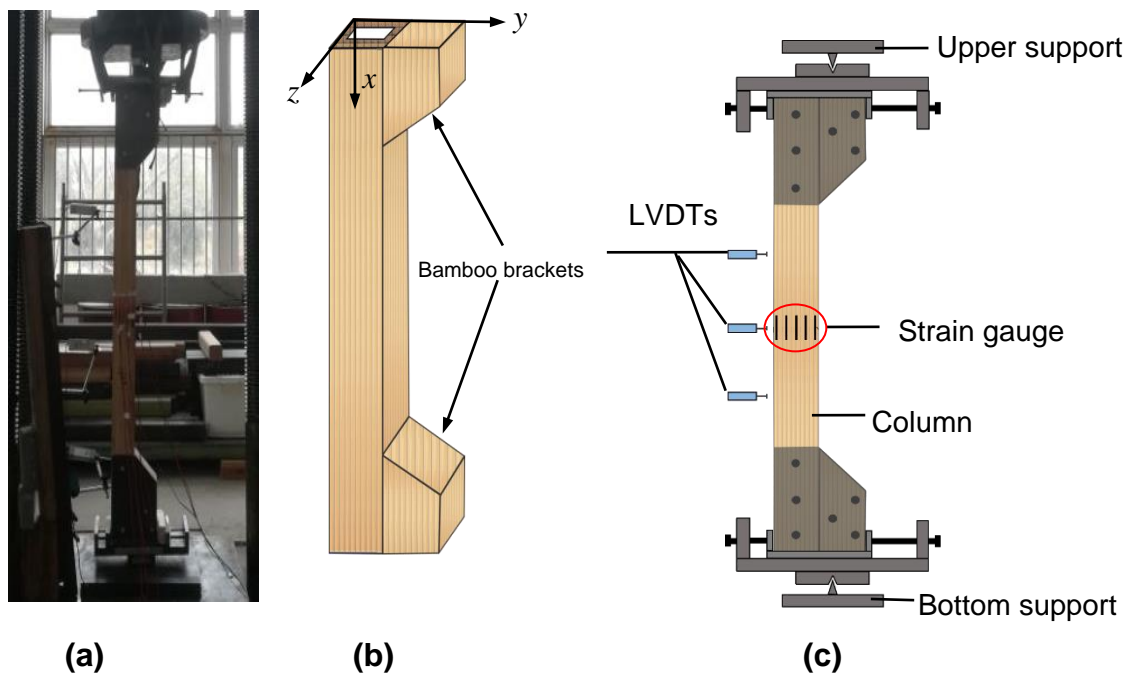


**Fig. 5.** Testing setup: (a) actual testing setup, (b) specimen, and (c) details of testing setup

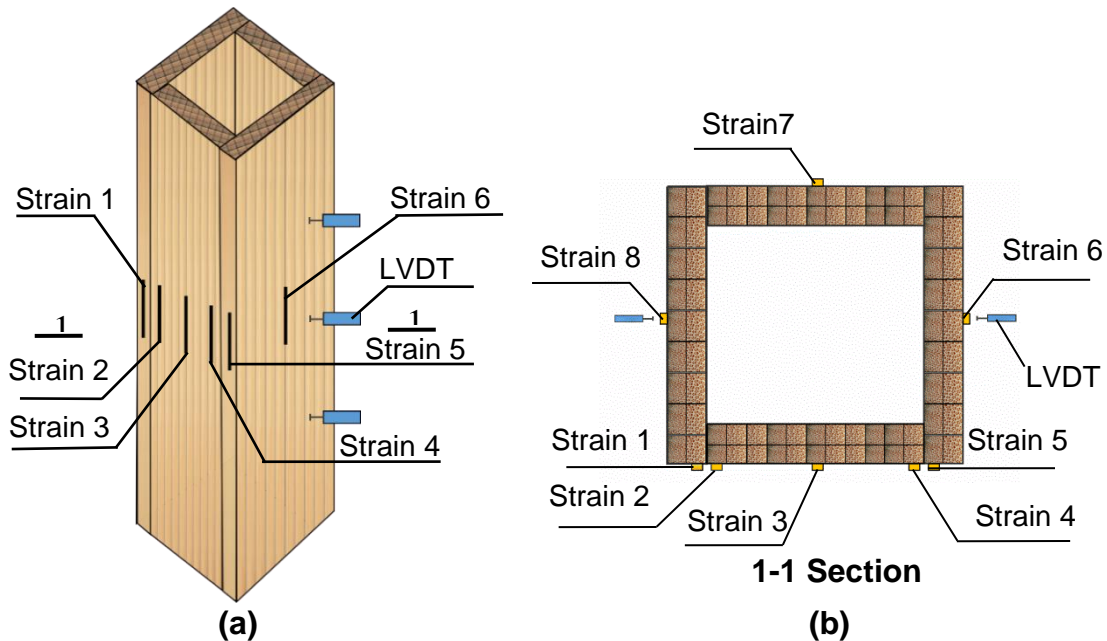


**Fig. 6.** Diagram of strain gauges and LVDTs: (a) measuring points; (b) cross-section diagram

To verify the plane-section assumption, strain gauges 1, 2, 3, 4, and 5 were placed at the side plate. Strain gauges 3, 6, 7, and 8 were placed in the middle of the four plates. All strain gauges were 50 mm × 3 mm. At first, a load of 0.5 kN was applied for 5 min to check instruments. The strain values of 3, 6, 7, and 8 were compared, and the position of the specimen was adjusted until the error of the strain gauges was small. The LVDTs were placed on the endplates, as shown in Fig. 6. The load cell, strain gauge, and LVDTs were connected to the TDS-530, and the acquisition frequency was 10 Hz.

## RESULTS AND DISCUSSION

### Failure Modes

During the loading of the long column, there was no obvious deformation in the initial loading stage. When the load increased to 50% of the peak load, lateral deformations were observed, as shown in Fig. 7(a). The lateral displacement curves were linear, which indicated that the hollow column was in the elastic stage at this time. As the load continuously increased, when the load increased to 60% of the peak load, the cracks occurred on the surface of the column at the mid-span, as shown in Fig. 7(b), and a "crackling" sound was heard at the same time. When the load increased to the peak load, the lateral displacement curves began to decline slowly. The lateral deformation increased quickly, and cracks occurred near the bamboo brackets. The cracks continued to expand to the mid-span section, as shown in Fig. 7(c). Finally, the fibers on the tensioned side were broken, as shown in Fig. 7(d).

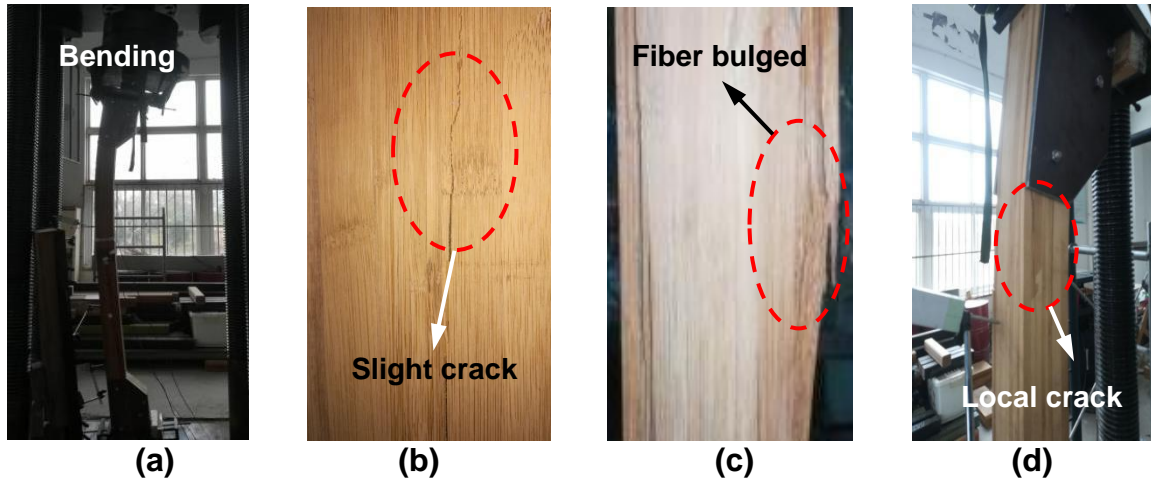


**Fig. 7.** Failure modes of a long column: (a) buckling, (b) crack, (c) fiber bulged failure, and (d) local crack

In the intermediate column, the lateral deformation was very small in the initial stage. When the load increased to 40% of the peak load, a slight lateral deformation was observed, as shown in Fig. 8(a). The column remained in the elastic stage. When the load was increased, the lateral deformation became larger, and the cracking sound was heard intermittently. Local cracks occurred at the glued places of the plates, as shown in Fig. 8(b). When the load increased to 60% of the peak load, the lateral deformation became more obvious. The lateral displacement curves no longer maintained linear, and the strain on the compressive side had exceeded the proportional ultimate compressive strain, which indicated that the column entered the elastoplastic stage. As the load continuously increased, the lateral deformation of the specimen was became larger. Cracks near the bamboo brackets occurred, and the cracks were expanded to the mid-span section, as shown in Fig. 8(c). When the load reached the peak load, the fibers on the tensile side were broken with a “snap” sound, as shown in Fig. 8(d). The load began to drop, and the strain on the tensile side almost reached the ultimate tensile strain, and then the test was stopped.

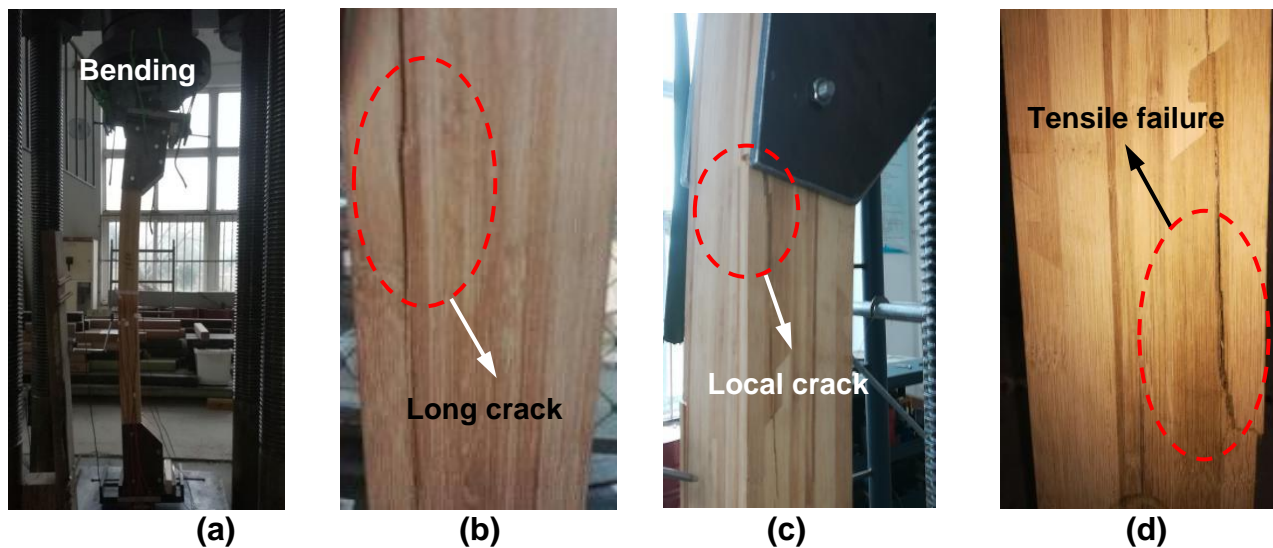


**Fig. 8.** Failure modes of intermediate column: (a) buckling, (b) long crack, (c) local crack, and (d) tensile failure

## Test Results and Analysis

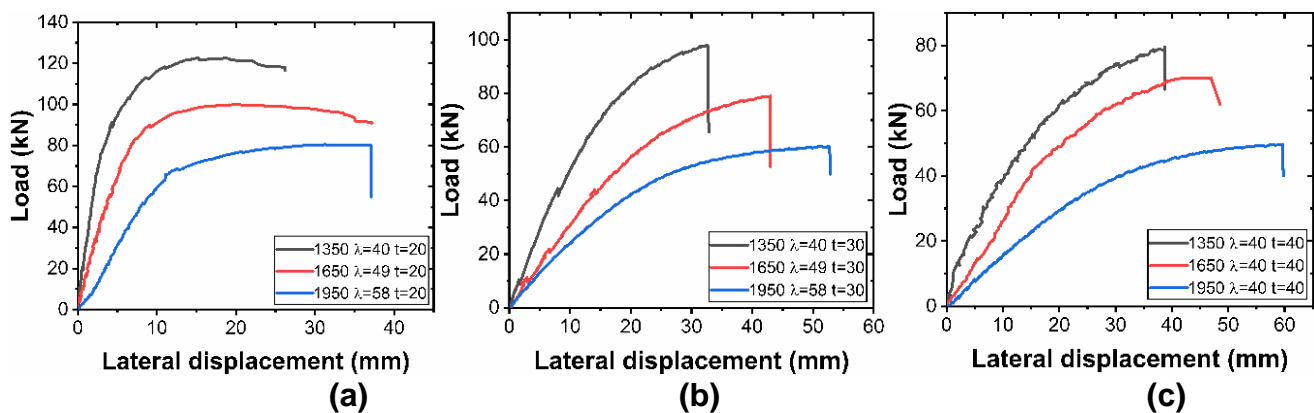
The test results of GLBHC under eccentric compression are shown in Table 3.

**Table 3.** The Results of GLBHC under Eccentric Compression

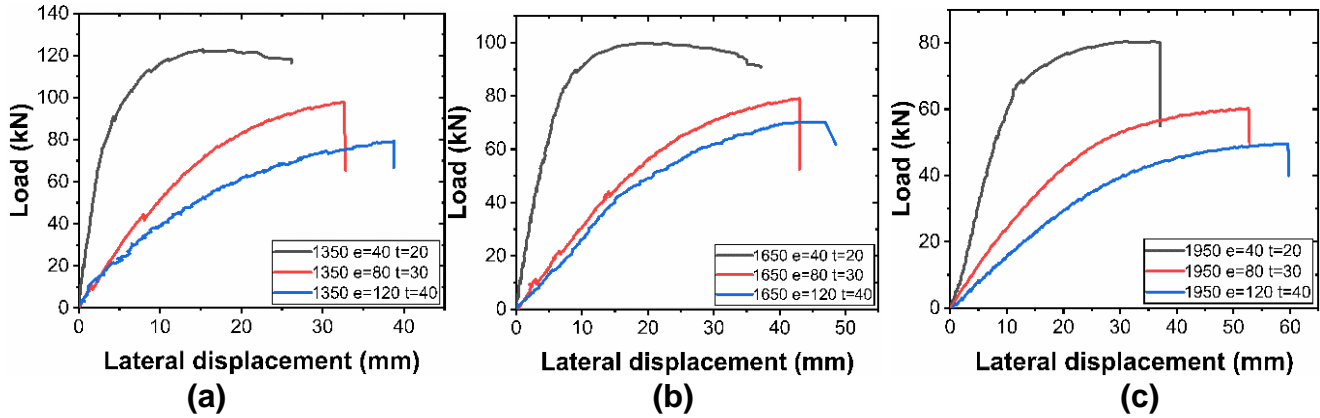
Specimens	Slenderness ratio	$e/mm$	$t/mm$	$P_u/kN$	$y/mm$
1350-40	40	40	20	122.28	18.64
1350-80	40	80	30	97.71	32.64
1350-120	40	120	40	79.37	38.74
1650-40	49	40	20	99.73	22.54
1650-80	49	80	30	80.05	42.99
1650-120	49	120	40	70.35	46.89
1950-40	58	40	20	80.32	35.77
1950-80	58	80	30	60.24	51.21
1950-120	58	120	40	49.59	59.64

The lateral displacement curves are shown in Figs. 9 and 10. In Fig. 9, the ultimate bearing capacity of GLBHCs decreased with the slenderness ratio increasing, which have the same eccentric distance and wall thickness. In Fig. 10, the ultimate bearing capacity decreases with the eccentric distance increasing when they have the same slenderness ratios. When the wall thickness increases, its ultimate bearing capacity should be increased according to the Euler theory. But it is also affected by the eccentric distance.

When the eccentric distance increases, its ultimate bearing capacity was decreased, which indicates that eccentric distance is the reason for the reduction of the ultimate bearing capacity for GLBHCs.



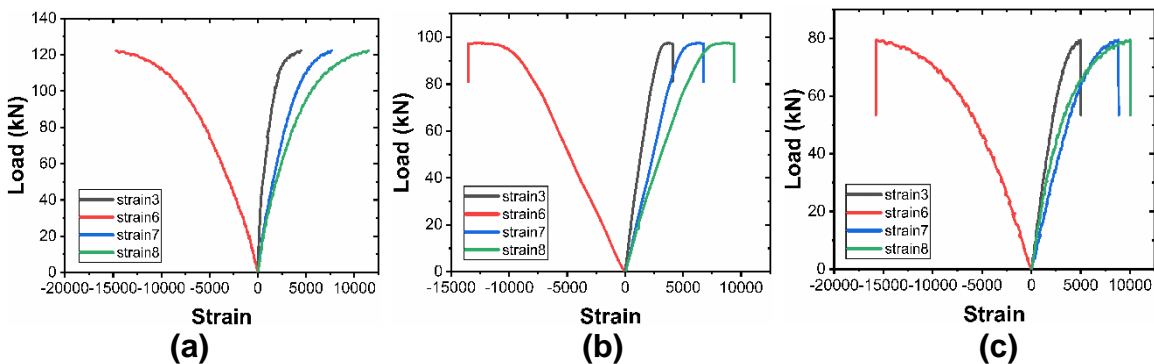
**Fig. 9.** The effects of eccentric distances on its ultimate bearing capacity: (a)  $e=40$ ; (b)  $e=80$ ; (c)  $e=120$



**Fig. 10.** The effects of slenderness ratios and wall thicknesses on its ultimate bearing capacity: (a)  $\lambda = 40$  (b)  $\lambda = 49$  (c)  $\lambda = 58$

The load-strain curves in Fig. 11 show that: (1) the load-strain curves of each specimen are similar; (2) in the initial loading stage, the load-strain curves were linear, which indicates that the column is in the elastic stage. After that, the curves began to bend slightly, which indicates that the column entered the elastoplastic stage. When the column had a small eccentric distance, its load dropped slowly after reaching the peak load. Conversely, for the column with a large eccentric distance, the load dropped quickly; (3) a larger eccentric distance resulted in a smaller ultimate bearing capacity.

The mid-span cross-sectional strain curves are shown in Fig. 12. The cross-sectional strain curves remained linear before the column failed, which indicates that the glued connections of the plates were not broken and its cross-sectional strain complied with the flat section assumption. As the load increased, the position of the neutral axial was biased toward the compressive zone because the compressive elastic modulus was greater than the tensile elastic modulus. A larger eccentric distance resulted in a greater bias.



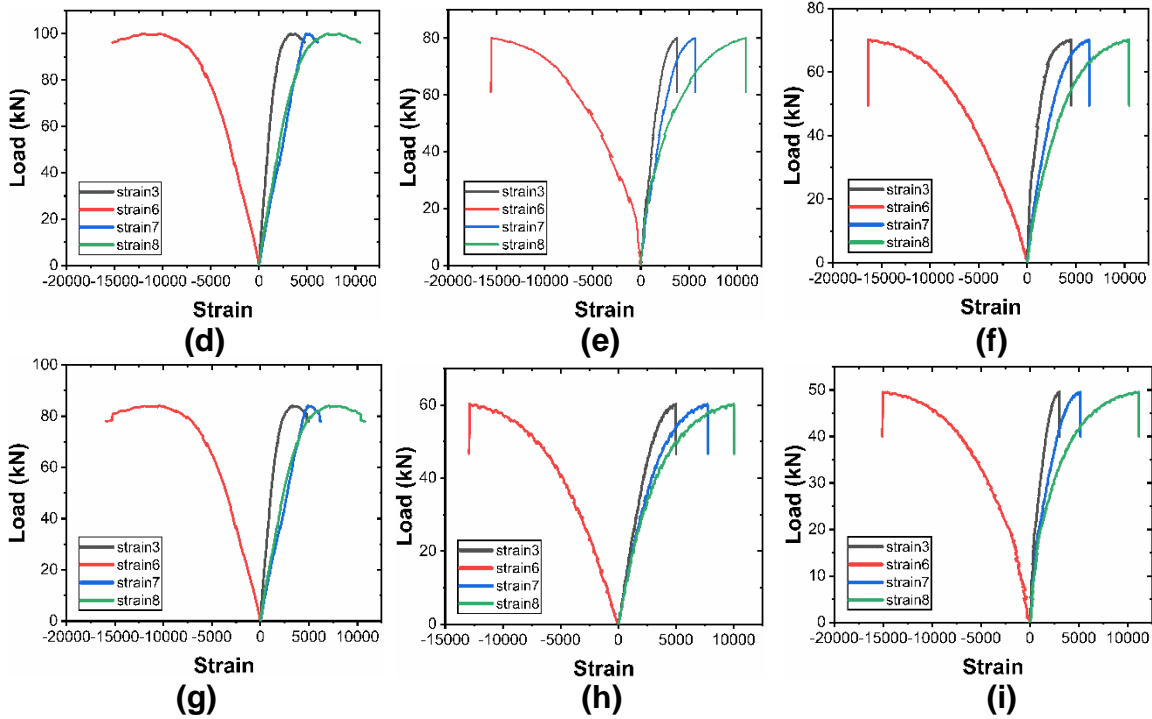


**Fig. 11.** Load-strain curves: (a)1350-40 (b)1350-80 (c)1350-120 (d)1650-40 (e)1650-80 (f)1650-120 (g)1950-40 (h)1950-80 (i)1950-120

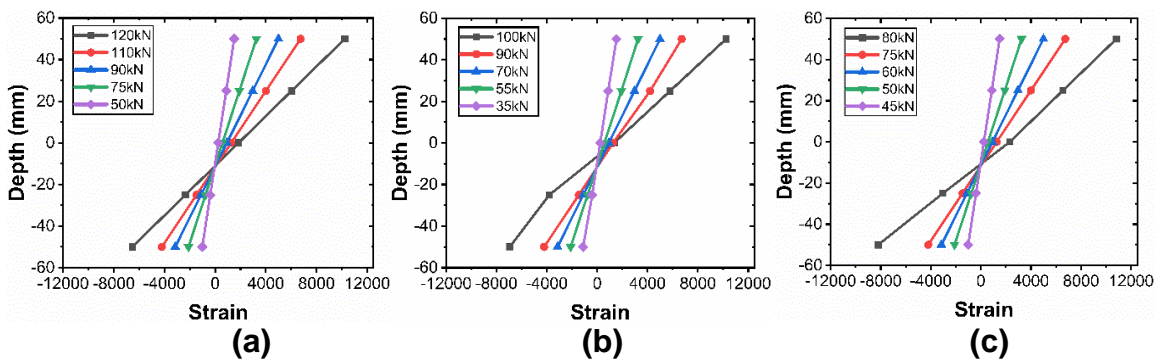


**Fig. 12.** Mid-span cross-sectional strain curves: (a)1350-40 (b)1350-80 (c)1350-120

### Ultimate Bearing Capacity

The elastoplastic buckling of GLBHC occurs under the eccentric load. The P-delta effect (Medri 1982) and the differences in tensile and compressive elastic modulus (Yao *et al.* 2004) have a great effect on its ultimate bearing capacity. To consider these factors, a new ultimate bearing capacity model is proposed based on the elastic small deformation theory.

### Mid-span Lateral Displacement

The lateral displacement curves are shown in Fig. 13, where three LVDTs are set on the tensile side of the specimens. At the knife hinges, the lateral displacement is zero. The shape of these curves is similar. Under the same slenderness ratio, the lateral displacement is larger with increasing eccentric distance. When the eccentric distance is the same, the larger slenderness ratio results in greater lateral displacement but lower the ultimate bearing capacity.

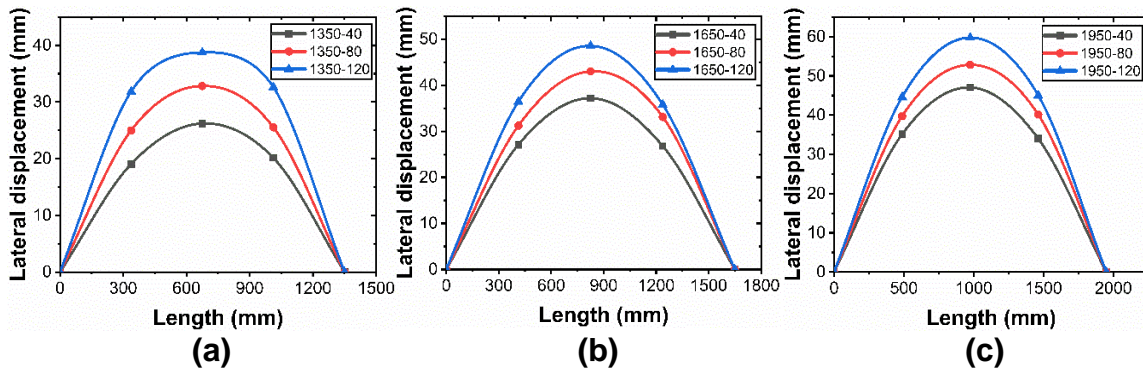


**Fig. 13.** Lateral displacement curves: (a) column(L=1350), (b) column(L=1650), and (c) column(L=1950)

The common forms of equations for deflection curves include quadratic polynomial function, half-wave sine function, half-wave cosine function, *etc.* (Hong *et al.* 2021; Zhou *et al.* 2022). The fitting curves with quadratic polynomial functions and sinusoidal functions are shown in Figs. 14(a) and 14(b). There were local errors between them. Furthermore, the average value of them was closer to the test value, as shown in Fig. 14(c).

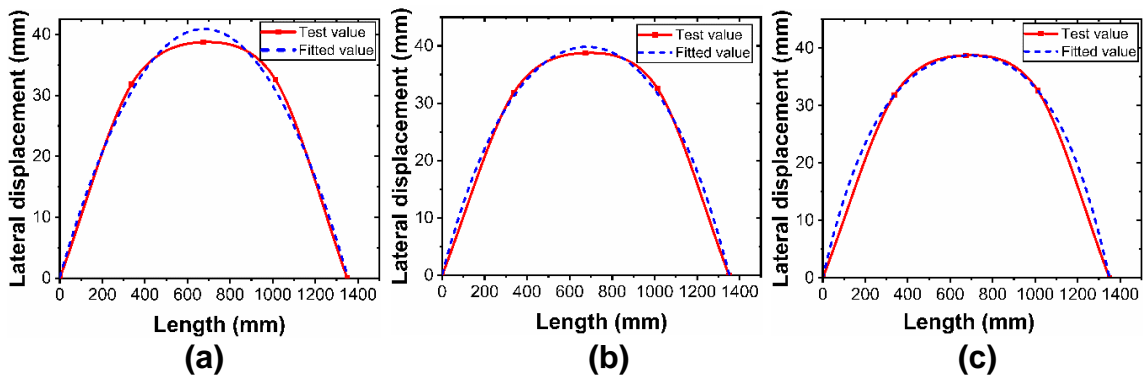


**Fig. 14.** The deflection curves of the column: (a) quadratic polynomial function, (b) half-wave sine function, (c) average function

The deflection of the hollow column under eccentric pressure is related to the curvature radius of the section ( $\rho$ ), which is calculated as follows,

$$\frac{1}{\rho} = \left| \frac{y''}{(1+y')^{3/2}} \right| = \frac{2a}{[1+a(l-2x)]^{3/2}} \tag{4}$$

where  $y$  is the lateral displacement at any point of the column,  $a$  is coefficient of the deflection curves,  $x$  is the distance from the end of the column, and  $l$  is the length of the column.

The equation for the quadratic function and sine function deflection curves can be set as follows,

$$v = a(-x^2 + lx) \tag{5}$$

$$w = a \sin \frac{\pi x}{l}, (0 \leq x \leq l) \quad (6)$$

where  $v$  and  $w$  are the deflections of quadratic and sinusoidal functions, respectively. Taking the average of the mid-span lateral displacement of the sine and quadratic functions, the equation for mid-span lateral displacement of the GLBHC is as follows,

$$y_{\max} = \frac{8 + \pi^2}{16\pi^2} \frac{l^2}{\rho} \quad (7)$$

where  $y_{\max}$  is the lateral maximum displacement of the mid-span section.

The eccentric load can be equated to the combined action of the bending moment and the axial force, which can be used to establish the equilibrium equation of force and bending moment. The GLBHC can be divided into two failure modes: (1) when the tensile strain reaches the ultimate tensile strain, it is called the large eccentric compressive failure; and (2) when the compressive strain reaches the ultimate compressive strain, it is called the small eccentric compressive failure. The specific derivation process is as follows (Huang *et al.* 2015).

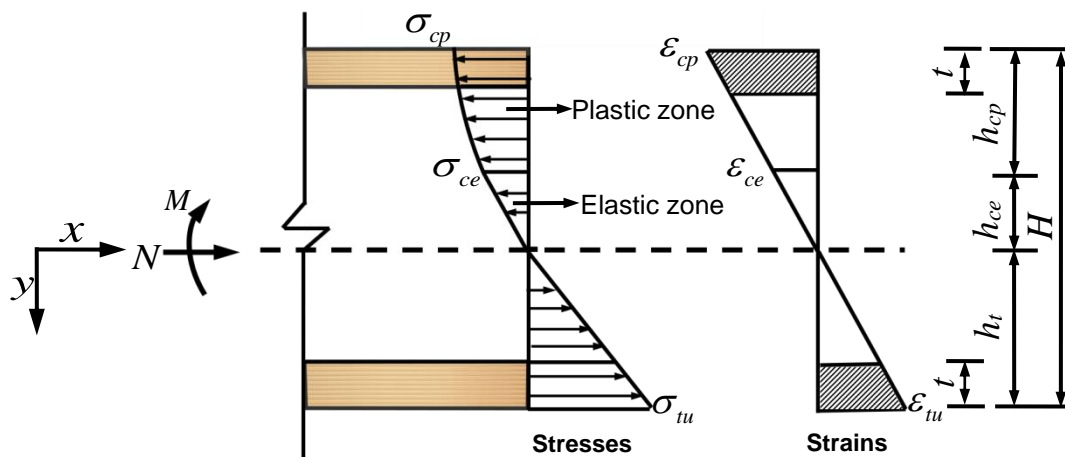


**Fig. 15** The model of the mid-span stress-strain under the large eccentric load

*Large eccentric model*

The model of the mid-span stress-strain relationship is shown in Fig. 15. The height of the section  $H$  can be divided into three zones, where  $h_{cp}$  is the height of the compressive plastic zone,  $h_{ce}$  is the height of the compressive elastic zone, and  $h_t$  is the height of the tensile zone. Because it is a large eccentric compression model, the tensile zone reaches the ultimate tensile strain  $\varepsilon_{tu}$ , and the compressive elastic zone and the compressive plastic zone are divided by the proportional ultimate strain  $\varepsilon_{ce}$ . The strains at the compression edge do not reach the ultimate compressive strain. With the neutral axis as the x-axis and the cross-section height as the y-axis, the tensile side as the positive direction, and the compressive side as the negative direction, as shown in Fig. 15, the curvature  $k$  of the mid-span section can be expressed as follows,

$$k = \frac{1}{\rho} = \frac{\varepsilon_{tu}}{h_t} = \frac{-\varepsilon_{ce}}{h_{ce}} = \frac{-\varepsilon_{cp}}{h_{ce} + h_{cp}} \quad (8)$$

Substituting the relevant mechanical properties parameters of the material into Eq. 8, one obtains:

$$h_t = \frac{-\varepsilon_{tu}}{\varepsilon_{ce}} h_{ce} = \frac{0.0118}{0.0033} h_{ce} = 3.6h_{ce} \quad (9)$$

Substituting  $\varepsilon = ky$  into the stress-strain relationship model,

$$\sigma(\varepsilon) = \begin{cases} E_t ky & 0 \leq y \leq h_t \\ E_c ky & -h_{ce} \leq y \leq 0 \\ a_1 k^2 y^2 + b_1 ky + c_1 & -(h_{cp} + h_{ce}) \leq y \leq -h_{ce} \end{cases} \quad (10)$$

where  $E_t$  is the elastic tensile modulus,  $E_c$  is elastic compressive modulus, and  $a_1$ ,  $b_1$ , and  $c_1$  are the mechanical properties parameters of the material. According to Fig. 15,

$$h_t + h_{ce} + h_{cp} = H \quad (11)$$

Assuming that the cross-section width is denoted by  $B$ , the equation is established based on the balance of force and bending moment, as follows.

$$\begin{cases} \int_{h_t-t}^{h_t} E_t ky dy + \int_{-(h_{cp}+h_{ce})}^{-(h_{cp}+h_{ce}-t)} (ak^2 y^2 + bky + c) dy = \frac{N}{B} \\ \int_{h_t-t}^{h_t} E_t ky^2 dy + \int_{-(h_{cp}+h_{ce})}^{-(h_{cp}+h_{ce}-t)} (ak^2 y^2 + bky + c) y dy = \frac{M}{B} \end{cases} \quad (12)$$

The stress-strain relationship is as follows.

$$\begin{cases} \sigma_{tu} = E_t kh_t \\ \sigma_{ce} = -E_c kh_{ce} \end{cases} \quad (13)$$

Equation 12 can be simplified by substituting Eqs. 8, 9, 10 and 13 into the terms to obtain Eq. 14.

$$\left\{ \begin{aligned} & \left( 119.02t - \frac{16.53t^2}{h_{ce}} \right) + \frac{0.37}{h_{ce}^2} \left[ (H - 5.6h_{ce})^3 - (H - 3.6h_{ce} - t)^3 \right] + 70.13t + \\ & \frac{6.06(t^2 - 2Ht)}{h_{ce}} = \frac{N}{B} \\ & \frac{11.02}{h_{ce}} \left[ 46.66h_{ce}^3 - (3.6h_{ce} - t)^3 \right] + \frac{0.28}{h_{ce}^2} \left[ (H - 3.6h_{ce} - t)^4 - (H - 3.6h_{ce})^4 \right] \\ & + \frac{4.04}{h_{ce}} \left[ (H - 3.6h_{ce})^3 - (H - 3.6h_{ce} - t)^3 \right] - 95.4h_{ce} - 13.25t + 26.5H = \frac{M}{B} \end{aligned} \right. \quad (14)$$

*Small eccentricity model*

The model of the mid-span stress-strain relationship is shown in Fig. 16.

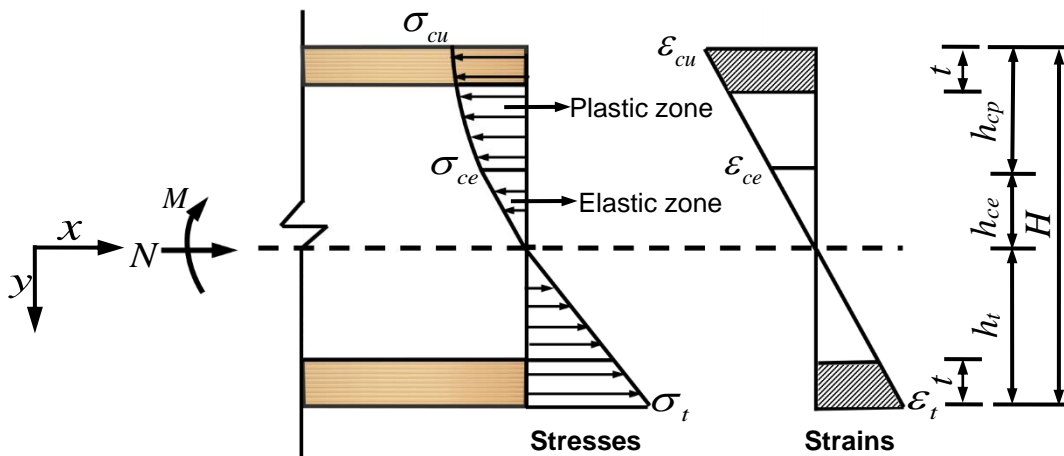


**Fig. 16.** Model of the mid-span stress-strain under the small eccentric load

In Fig. 16, the edge strain of the compressive zone reaches the ultimate compressive strain  $\epsilon_{cu}$ , which is different from the large eccentric model, and the strains at the tensile edge do not reach the ultimate tensile strain  $\epsilon_{tu}$ . Based on the analysis steps of the large eccentric model, Eq. 15 is obtained.

$$\left\{ \begin{aligned} & k = \frac{-\epsilon_{ce}}{h_{ce}} = \frac{-\epsilon_{cu}}{h_{ce} + h_{cp}} = \frac{\epsilon_t}{h_t} \\ & h_{cp} = 4.42h_{ce} \end{aligned} \right. \quad (15)$$

Equation 12 can be simplified by substituting Eqs. 11, 13, and 15 into the terms to obtain Eq. 16.

$$\left\{ \begin{aligned} & \frac{59.5t}{H-5.42h_{ce}}(2H-t-10.84) + \frac{0.37}{h_{ce}^2} [29.38h_{ce}^3 - (5.42h_{ce}-t)^3] - 92.19t \\ & + \frac{6.06t^3}{h_{ce}} = \frac{N}{B} \\ & \frac{39.67}{H-5.42h_{ce}} [(H-5.42h_{ce})^3 - (H-5.42h_{ce}-t)^3] + 1443.63th_{ce} - 13.25t^2 + \\ & \frac{0.28}{h_{ce}^2} [(5.42h_{ce}-t)^4 - 862.97h^4] + \frac{4.04}{h_{ce}} [159.22h_{ce}^3 - (5.42h_{ce}-t)^3] = \frac{M}{B} \end{aligned} \right. \quad (16)$$

The ratio of the height of the compressive zone to the height of the cross-section is denoted by  $\alpha$ . Its value can be determined according to the Eqs. 8, 9, 11, and 15, where  $\alpha = (h_{ce} + h_{cp}) / H$ . When the tensile strain and compressive strain all reach the ultimate strain,  $\alpha$  is 0.7120, which can be used to determine whether the column is a large eccentric model or a small eccentric model.

The corresponding critical load  $N$  can be obtained by substituting  $\alpha$ ,  $B$ ,  $t$ , and  $H$  into Eqs. 14 and 16, and its value is  $9.8BH$ . When  $N \geq 9.8BH$ , it is a small eccentric compressive failure; otherwise it is a large eccentric compressive failure.

The corresponding bending moment  $M$  can be obtained by substituting the load  $N$  into Eqs. 14 and 16. Equation 17 can be established based on the balance of the bending moment.

$$M = N(e + y_{\max}) = M_0 + M_1 \quad (17)$$

where  $e$  is the eccentric distance,  $y_{\max}$  is the mid-span deflection,  $M$  is the bending moment at the end of the column,  $M_0$  is the equivalent bending moment generated by the the eccentric distance, and  $M_1$  is the bending moment generated by the P-delta effect.

Substituting Eqs. 7 and 8 into Eqs. 17, Eqs. 17 is obtained.

$$M = M_0 + \frac{8+\pi^2}{16\pi^2} \cdot \frac{\varepsilon_{ce} l^2 N}{\alpha H} \quad (18)$$

The formula for the ultimate bearing capacity of GLBHC under the eccentric compression  $P_{cr}$  can be expressed as follows.

$$P_{cr} = \frac{M_0}{e} + \frac{8+\pi^2}{16\pi^2} \cdot \frac{\varepsilon_{ce} l^2 N}{\alpha H e} \quad (19)$$

## Validation

Specimens with the cross-section size (100 mm × 100 mm) and wall thickness ( $t = 20$  mm) were selected. The theoretical results of the GLBHC with column lengths of 1350 mm, 1650 mm, and 1950 mm are shown in Table 4. Errors between the theoretical results and test values were less than 10%, which indicates the formula can well estimate the ultimate bearing capacity of GLBHC under the eccentric compression. The theoretical and test results are in Fig. 17.

**Table 4.** The Calculated Results of the Selected Column

1350 mm			1650 mm			1950 mm		
N (kN)	M (kN·m)	$\alpha$	N (kN)	M (kN·m)	$\alpha$	N (kN)	M (kN·m)	$\alpha$
20	11.21	0.9996	20	10.92	0.9996	20	10.24	0.9996
40	11.04	0.8962	30	10.67	0.9251	25	9.31	0.9540
60	10.23	0.8012	40	10.17	0.8962	30	9.04	0.9251
80	9.51	0.7242	50	9.47	0.8513	35	8.74	0.9136
98	7.92	0.7120	60	9.08	0.8012	40	7.63	0.8962
100	7.82	0.7267	70	8.24	0.7588	45	6.96	0.8044
120	6.07	0.7499	80	7.12	0.7242	50	6.39	0.8513
140	4.25	0.7678	90	5.68	0.7171	55	5.82	0.8237
160	0.43	0.7871	98	4.26	0.7120	60	5.03	0.8012
			100	3.42	0.7267	65	4.31	0.7839
			110	0.21	0.7409	70	3.12	0.7588
						75	1.35	0.7409
						80	0.33	0.7242

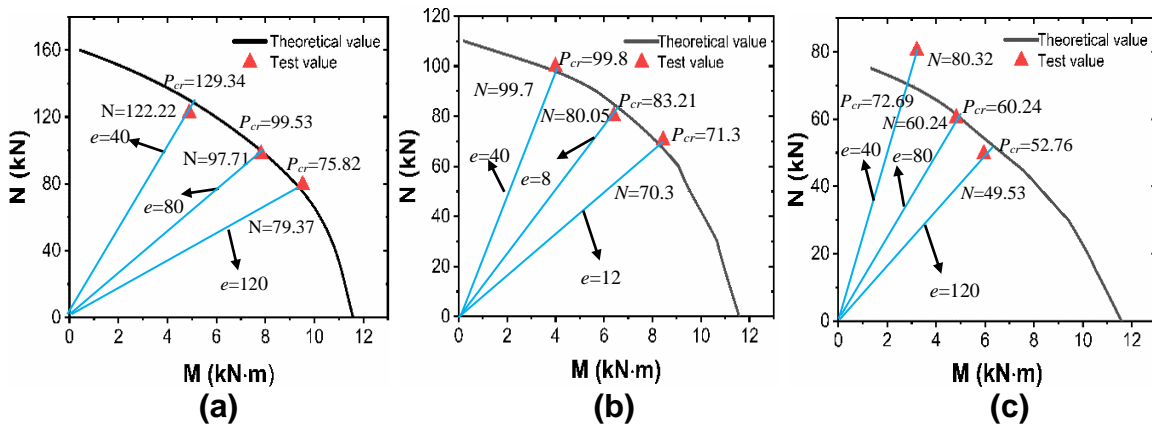


**Fig. 17.** Comparison between theoretical and test values: (a) 1350 mm, (b) 1650 mm, (c) 1950 mm

**CONCLUSIONS**

1. In this paper, the ultimate bearing capacity of glue-laminated bamboo hollow columns (GLBHC) under eccentric compression was studied and it can be divided into a long column, intermediate column, and short column. Their failure modes are different and are related to the slenderness ratios. The elastic buckling occurs in the long column and the elastoplastic buckling occurs in the intermediate column. Under the same slenderness ratio, the lateral displacement is larger with the eccentric distance increasing. When the eccentric distance is the same, the larger the slenderness ratio, the greater the lateral displacement, but the lower the ultimate bearing capacity. Therefore, eccentric distance is the main reason for the reduction of the ultimate bearing capacity.
2. The cross-sectional strain remains linear before the hollow column fails, which is the basis for adopting the flat section assumption. Due to the differences in tensile and compressive elastic modulus, the position of the neutral axial is biased toward the compressive zone.

3. To accurately estimate the ultimate bearing capacity of GLBHC under eccentric compression, one can take the strains at the edge reach the ultimate strain as the failure criterion. Two calculation models under the eccentric compression are established based on the balanced equation of force and bending moment, which considers the differences in tensile and compressive elastic modulus and elastic-plastic deformation. The formula for the ultimate bearing capacity of GLBHC under the eccentric compression is derived. As a result, the test results are in good agreement with the theoretical results.

## FUTURE WORK

In this paper, a formula for estimating the ultimate bearing capacity of GLBHC under eccentric compression was proposed and it was found that the test results were in good agreement with the calculated results. However, there are still some valuable problems requiring to be further studied in future work. For example, the bamboo properties will change with respect to the distance from the tangential outer surface as one moves inwards, which is not considered in this paper. So it is valuable to study the changeable bamboo properties on its ultimate bearing capacity in future work.

## ACKNOWLEDGEMENTS

The authors thank Nanjing Forestry University for the test equipment and for providing the scholarship award to carry out the research project.

## REFERENCES CITED

- AlAjarmeh, O. S., Manalo, A. C., Benmokrane, B., Karunasena, W., Mendis, P., and Nguyen, K. T. (2019). "Compressive behavior of axially loaded circular hollow concrete columns reinforced with GFRP bars and spirals," *Construction & Building Materials* 194, 12-23. DOI: 10.1016/j.conbuildmat.2018.11.016
- ASTM D143 (2022). "Standard test methods for small clear specimens of timber," West Conshohocken, USA.
- ASTM D198 (2022). "Standard test methods of static test of lumber in structural sizes," West Conshohocken, USA.
- Bahtiar, E. T., Malkowska, D., Trujillo, D., and Nugroho, N. (2021). "Experimental study on buckling resistance of *Guadua angustifolia* bamboo column," *Engineering Structures* 228, article no. 111548. DOI: 10.1016/j.engstruct.2020.111548
- Chen, Y., and Jin, L. (2020). "From continuous to snapping-back buckling: A post-buckling analysis for hyperelastic columns under axial compression," *International J. Non-Lin. Mechan.* 125, article no. 103532. DOI: 10.1016/j.ijnonlinmec.2020.103532
- Chen, F., Jiang, Z., Deng, J., Wang, G., Zhang, D., Zhao, Q., Cai, L., and Shi, S. Q. (2014). "Evaluation of the uniformity of density and mechanical properties of bamboo-bundle laminated veneer lumber (BLVL)," *BioResources* 9(1), 554-565. DOI: 10.15376/biores.9.1.554-565

- Chen, C., Li, H., Zhou, K., Dauletbek, A., Xiong, Z., Lorenzo, R., and Ashraf, M. (2022). "Behavior of CFRP-strengthened chamfered laminated bamboo lumber under eccentric compression," *Journal of Composites for Construction* 26(2), article no. 04022009. DOI: 10.1061/(ASCE)CC.1943-5614.0001197
- Danesh, F., and Mohammadrezapour, E. (2018). "Experimental investigation of T-stub link-to-column connections in eccentrically braced frames," *International Journal of Steel Structures* 18(2), 486-495. DOI: 10.1007/s13296-018-0017-y
- Dauletbek, A., Li, H., Xiong, Z., and Lorenzo, R. (2021). "A review of mechanical behavior of structural laminated bamboo lumber," *Sustainable Structures* 1(1), article no. 000004. DOI: 10.54113/j.sust.2021.000004
- GB/T 50329-2012 (2012). "Wood structure test method standard," Standardization Administration of China, Beijing, China.
- Guan, X., Yin, H., Liu, X., Wu, Q., and Gong, M. (2018). "Development of lightweight overlaid laminated bamboo lumber for structural uses," *Construction & Building Materials* 188(NOV.10), 722-728. DOI: 10.1016/j.conbuildmat.2018.08.107
- Harries, K. A., Petrou, M. F., and Brooks, G. (2000). "Structural characterization of built-up timber columns," *Journal of Architectural Engineering* 6(2), 58-65. DOI: 10.1061/(ASCE)1076-0431(2000)6:2(58)
- He, X. (2007). *Study on Nonlinear Mechanical Behavior of Elastic Structure*, Chongqing University, Chongqing, China.
- Hong, C., Li, H., Xiong, Z., Lorenzo, R., Corbi, I., and Corbi, O. (2021). "Experimental and numerical study on eccentric compression properties of laminated bamboo columns with a chamfered section," *Journal of Building Engineering* 43, article no. 102901. DOI: 10.1016/j.job.2021.102901
- Hu, H. S., Xu, L., Guo, Z. X., and Shahrooz, B. M. (2020). "Behavior of eccentrically loaded square spiral-confined high-strength concrete-filled steel tube columns," *Engineering Structures* 216, article no. 110743. DOI: 10.1016/j.engstruct.2020.110743
- Huang, D., Bian, Y., Huang, D., Zhou, A., and Sheng, B. (2015). "An ultimate-state-based-model for inelastic analysis of intermediate slenderness PSB columns under eccentrically compressive load," *Construction & Building Materials* 94, 306-314. DOI: 10.1016/j.conbuildmat.2015.06.059
- Li, H, Zhang Q, Wu G, Xiong X, and Li Y. (2016). "Research progress of bamboo integrated materials," *Forestry Engineering Journal* 1(06), 10-16. (In Chinese) DOI: 10.13360/j.issn.2096-1359.2016.06.002
- Li, H. T., Chen, G., Zhang, Q., Ashraf, M., Xu, B., and Li, Y. (2016). "Mechanical properties of laminated bamboo lumber column under radial eccentric compression," *Construc. Building Mater.* 121, 644-652. DOI: 10.1016/j.conbuildmat.2016.06.031
- Li, Z., He, M., Tao, D., and Li, M. (2016). "Experimental buckling performance of scrimber composite columns under axial compression," *Composites Part B: Engineering* 86, 203-213. DOI: 10.1016/j.compositesb.2015.10.023
- Liu, Y., Tang, S., Guo, Y., Xiao, Z., and Su, X. (2020). "Axial compression of three types of bamboo scrimber columns with different cross-sections," *BioResources* 15(4), 8093-8109. DOI: 10.15376/biores.15.4.8093-8109
- Medri, G. (1982). "A nonlinear elastic model for isotropic materials with different behavior in tension and compression," *Journal of Engineering Materials and Technology* 104(1), 26-28. DOI: 10.1115/1.3225031

- Mena, J., Vera, S., Correal, J. F., and Lopez, M. (2012). "Assessment of fire reaction and fire resistance of *Guadua angustifolia kunth* bamboo," *Construction and Building Materials* 27(1), 60-65. DOI: 10.1016/j.conbuildmat.2011.08.028
- Nie, Y., Wei, Y., Huang, L., Liu, Y., and Dong, F. (2021). "Influence of slenderness ratio and sectional geometry on the axial compression behavior of original bamboo columns," *Journal of Wood Science* 67(1), 1-20. DOI: 10.1186/s10086-021-01968-6
- Sharma, B., Gatóo, A., and Ramage, M. H. (2015). "Effect of processing methods on the mechanical properties of engineered bamboo," *Construction & Building Materials* 83, 95-101. DOI: 10.1016/j.conbuildmat.2015.02.048
- Sui, W., Cheng, H., and Wang, Z. (2018). "Bearing capacity of an eccentric tubular concrete-filled steel bridge pier," *Steel & Composite Structures, An International Journal* 27(3), 285-295. DOI:10.12989/scs.2018.27.3.285
- Tan, C., Li, H., Wei, D., Lorenzo, R., and Yuan, C. (2020). "Mechanical performance of parallel bamboo strand lumber columns under axial compression: Experimental and numerical investigation," *Construction & Building Materials* 231, article no. 117168. DOI: 10.1016/j.conbuildmat.2019.117168
- Varela, S., Correal, J., Yamin, L. E., and Ramirez, F. (2013). "Cyclic performance of glued laminated *Guadua* bamboo-sheathed shear walls," *Journal of Structural Engineering* 139(11), 2028-2037. DOI: 10.1061/(ASCE)ST.1943-541X.0000758
- Wang, C., Zhang, H., Zhao, C., Zhang, C., Cao, T., Dong, H., Ding, J., Xiong, Z., Xiong, X., Yan, Z., *et al.* (2018). "Experimental study on laminated bamboo lumber column," *In E3S Web of Conferences* 38(1), article no. 02001. DOI: 10.1051/e3sconf/20183802001
- Wang, X., Zhou, A., Zhao, L., and Chui, Y. H. (2019). "Mechanical properties of wood columns with rectangular hollow cross section," *Construction and Building Materials*, 214, 133-142. DOI: 10.1016/j.conbuildmat.2019.04.119
- Wu, F., Zheng, X. Y., and Ding, J. W. (2014). "Experimental study on performance of steel and composite plate combined column," in: *Advanced Materials Research* 919, 1805-1811. DOI: 10.4028/www.scientific.net/AMR.919-921.1805
- Yao, X., Peng, R., Du, C., Hua, Y., Zhang, J., Huang, Q., and Liu, H. (2019). "A two-step method for fabricating bamboo culm coated with MgAl-LDHs and its fire resistance properties," *Bioresources* 14(3), 5150-5161. DOI: 10.13360/j.issn.2096-1359.2016.01.010
- Zhao, W., Chen, Z., and Yang, B. (2017). "Axial compression performance of steel/bamboo composite column," *Procedia Engineering* 210, 18-23. DOI: 10.1016/j.proeng.2017.11.043
- Zhou, L., Liu, Q., Ma, S., and Han, X. (2021). "Eccentric compression behavior of long poplar columns externally reinforced by BFRP," *Journal of Wood Science* 67(1), 1-17. DOI: 10.1186/s10086-020-01934-8
- Zhou, K., Li, H., Dauletbek, A., Yang, D., Xiong, Z., Lorenzo, R., Zhou, K., Corbi, I., and Corbi, O. (2022). "Slenderness ratio effect on the eccentric compression performance of chamfered laminated bamboo lumber columns," *Journal of Renewable Materials* 10(1), 165. DOI: 10.32604/jrm.2022.017223

Zhu, H., Liu, J., and Wang, J. (2021). “Study on eccentric compression mechanical properties of plywood hollow column,” *Highway Engineering* 46(02), 71-76+88. (In Chinese) DOI: 10.19782/j.cnki.1674-0610.2021.02.012

Article submitted: June 14, 2022; Peer review completed: July 23, 2022; Revised version received and accepted: July 27, 2022; Published: July 29, 2022.  
DOI: 10.15376/biores.17.3.5372-5392